Clays and Clay Minerals, Vol. 61, No. 2, 141–151, 2013.

MAPPING KAOLINITE AND DICKITE IN SANDSTONE THIN SECTIONS USING INFRARED MICROSPECTROSCOPY

VALENTIN ROBIN*, SABINE PETIT, DANIEL BEAUFORT, AND DIMITRI PRÊT

Université de Poitiers, CNRS UMR 7285 IC2MP, HydrASA Bât. B35, rue Michel Brunet, F-86022 Poitiers Cedex, France

Abstract—A method to characterize and map both kaolinite and dickite polytypes in sandstone thin sections using infrared microspectroscopy (IRMS) was developed. Minerals identification using IRMS can be performed using the hydroxyl-stretching band of most clay minerals (3500−4000 cm^{-1}) in spite of infrared (IR) interferences caused by the embedding resin and glass substratum. Emphasis was placed on determining the optimum analytical conditions for IR data acquisition. The best data-acquisition parameters for Fourier-transform infrared (FTIR) measurements (*i.e.* spectra quality as a function of beam size and the number of scans) were obtained from a series of single spectra. Then, spatial resolution was explored as a function of the IR beam size (from 50 μm × 50 μm to 15 μm × 15 μm) and the step-scan interval (*i.e.* the distance between two successive analysis points). The IRMS measurements were performed on thin sections of materials characterized previously using scanning electron microscopy (SEM) and chemical analysis. Using IRMS, locations on the thin sections containing nearly pure dickite or kaolinite polytypes were identified and mapped. Most spectra collected using IRMS represented kaolin mineral aggregates rather than individual crystals, however, and mixing of kaolin polytypes was common at the spatial resolution of the IR beam size used. The spatial resolution of the IRMS was comparable to optical petrography and made possible the identification of areas on the thin section for further '*in situ*' investigation using other methods (*e.g.* microprobe, Laser Ablation Inductively Coupled Plasma Mass Spectrometry – LA-ICP-MS, *etc*.). Also, the use of blocky crystal morphology to identify dickite was questioned, as kaolinite with blocky habit was identified. Mineral mapping using IRMS seems particularly suited for investigating petrographic relationships between kaolinite and dickite in sandstone diagenesis, but could also be used for clay minerals in other rock types or soils.

Key Words—Dickite, IR Microspectroscopy, Kaolinite, Mineral Mapping, Sandstone.

INTRODUCTION

Over the last decade, most of the advances in quantitative petrology involved the extensive use of modern image-processing techniques providing quantitative measurements of the spatial heterogeneities of rocks (mineralogy, texture, porosity...). Such mapping methods are the primary means for determining the exact relationships between mineral species and pores for researchers attempting to model the dissolution-crystallization processes experienced by rocks over geological time periods and their resulting petrophysical properties. Several methods based on chemical element mapping (acquired using various techniques) have been proposed to build mineral mapping in clay-rich natural rocks or engineered materials (De Andrade *et al.*, 2006; Munoz *et al.*, 2006; Prêt *et al.*, 2010a, 2010b). These methods are limited by the fact that they do not identify and are not able to visualize the polytypes of clay minerals. Furthermore, any methods which allow the visualization of the petrographic relationships between dickite and kaolinite in thin sections of sedimentary rocks would be of major interest to those investigating the kaolinite-to-dickite transition, which is a marker of the thermal history of sandstones during silicoclastic diagenesis (Beaufort *et al.*, 1998; Ehrenberg *et al.*, 1993; Lanson *et al.*, 1996, 2002). Classical methods for identification of clay minerals from powders (X-ray diffraction, XRD, or FTIR spectroscopy on KBr pellets) do not allow for localization of kaolin polytypes within the rocks being examined. Using the morphology of the crystals observed using a scanning electron microscope, *i.e.* vermiform habit for kaolinite *vs.* blocky habit for dickite (McAulay *et al.*, 1994; Osborne *et al.*, 1994), remains a rather subjective approach which can be contradicted by transmission electron microscopy (TEM) investigations (Kameda *et al.*, 2008). Moreover, building maps from localized characterizations of kaolin polytypes obtained by the use of electron back-scattering diffraction (EBSD) on individual crystals (Kogure *et al.*, 2005) or TEM through a focused ion beam (Kogure *et al.*, 2005) is difficult.

IRMS of thin sections is classically used for the petrographic study of rocks. However, few works dealing with IRMS for *in situ* characterization of clays are available in the literature. A polarizing infrared microspectrometer was used for the study of OH configuration on single crystals of kaolinite and dickite (Johnston *et al.*, 1990) and of muscovite (Tokiwai and Nakashima, 2010). Kaolinite was characterized by

* E-mail address of corresponding author:
valentin.robin@univ-poitiers.fr
DOI: 10.1346/CCMN.2013.0610211

reflection-mode IRMS (Rintoul and Fredericks, 1995) but only one study has dealt with the use of IRMS to characterize kaolinite in petrographic thin sections (Beauvais and Bertaux, 2002).

In the present study, the mapping of clay minerals by IRMS from thin sections of rocks was accomplished for the first time. Kaolin polytypes in thin sections of sandstones were identified and mapped using IRMS. Efforts to determine the best analytical conditions (single spectrum and mapping parameters) to optimize data acquisition were emphasized. The effects of acquisition parameters on spectrum statistics (beam size and number of scans) were evaluated from a single-point analysis prior to optimization of map parameters (step scan as a function of beam size).

EXPERIMENTAL

Materials

The specimen analyzed in the present study was a thin section obtained from a core sample collected within the oil-bearing Middle Jurassic Brent Group sediments of the Froy hydrocarbon reservoir (Norwegian continental shelf, North Sea). The specimen consists of a fine- to medium-grained arkosic sandstone lithified during burial to a depth of 3200 m. This specimen (referred to as 25/2-13 3417.85m) belongs to the series of samples investigated to refine the kaolinite–dickite transformation mechanism in sandstone reservoirs (Cassagnabère, 1998; Kameda *et al.*, 2008; Lanson *et al.*, 2002). According to mineralogical analyses based on XRD, differential thermal analyses, and IR spectroscopy, Cassagnabère (1998) determined that the kaolin material extracted from this specimen consists of a mixture of dickite (85%) and kaolinite (15%). More information about the mineral sequence and the diagenetic processes experienced by this sandstone can also be found in Cassagnabère (1998).

Associated FTIR features of kaolinite/dickite specimens

The 3500–3750 cm^{-1} IR range is usually used to distinguish the kaolin minerals. The FTIR spectra of the three kaolin polymorphs are significantly different. At ambient temperature, kaolinite exhibits four bands in the OH-stretching region at ~3695, 3668, 3652, and 3620 cm^{-1}, noted as ν_1, ν_2, ν_3, and ν_4, respectively, while only three bands at 3710, 3655, and 3622 cm^{-1} are observed for dickite (Farmer and Russell, 1964; Farmer, 1998; Frost *et al.*, 1997; Frost and Van Der Gaast, 1997; Ledoux and White, 1964; Madejová *et al.*, 2010; Prost *et al.*, 1987). Only four OH groups are present in the kaolinite unit cell (Bish, 1993), but the one-to-one assignment of the ν_1, ν_2, ν_3, and ν_4 to these single OH groups is incorrect based on their dichroic behavior (Farmer, 1974; Johnston *et al.*, 1990). Accordingly, first-principles modeling (Balan *et al.*, 2001, 2005, 2010) attributed the ν_1, ν_2, and ν_3 bands to vibrations of the three inner-surface OH groups, with ν_1 corresponding to the in-phase stretching mode and ν_2 and ν_3 to the anti-phase stretching modes, the ν_4 band being due to vibrations of the inner hydroxyl. The origin of the OH-stretching bands of dickite is still debated (Balan *et al.*, 2010).

Empirically, the wavenumber and the relative absorbance of the structural OH-stretching bands are commonly used as indicators of order/disorder in kaolin minerals. Some crystalline defaults in kaolinite, mostly related to stacking faults, may lead to local dickite-like features and the ratio of the ν_2 and ν_3 relative integrated intensities are commonly used as an order or disorder index reflecting the 'dickitic' or monoclinic character of kaolinite (Brindley *et al.*, 1986; Farmer and Russell, 1964; Farmer, 1974; Farmer, 1998; Frost *et al.*, 1997; Frost and Van Der Gaast, 1997; Prost *et al.*, 1989). By increasing the resolution of the IR spectra of the OH groups, low-temperature spectra allow clearer identification of dickite- and nacrite-like local configurations in disordered kaolinite (Balan *et al.*, 2010; Johnston *et al.*, 1990, 2008; Prost *et al.*, 1987, 1989).

Increasing amounts of dickite in a kaolinite-dickite mixture can be proven by the following characteristics of the OH-stretching IR bands (Beaufort *et al.*, 1998): (1) the progressive shift of ν_1 from 3695 cm^{-1} to 3710 cm^{-1} accompanied decreasing intensity and band broadening; (2) the progressive disappearance of ν_2 at 3668 cm^{-1}, a slight shift to 3655 cm^{-1} of the band at 3652 cm^{-1}, and a slight shift to 3622 cm^{-1} of the band at 3620 cm^{-1} .

Instrumentation

Infrared radiation from a FTIR spectrometer was transmitted to a microscope with IR detectors, allowing FTIR analysis in parallel with observations in microscopy. This offers the unique advantage over classical FTIR techniques of allowing *in situ* measurements.

The IR spectra were recorded in petrographic thin sections using an IR source and a Cesium Iodide (CsI) beamsplitter from a Nicolet™ 6700 FTIR spectrometer (Waltham, Massachusetts, USA). The spectrometer was coupled with a Thermo Scientific Nicolet™ Continuum FTIR microscope equipped with a Mercury Cadmium Telluride (MCT) detector cooled with liquid nitrogen. Analyses were collected in transmission mode in the middle infrared (MIR) domain between 4000 and 400 cm^{-1}. The IR beam from the spectrometer was transmitted to the microscope and was shaped by passing through a mask made of adjustable slits. The shaped IR beam was then passed through samples and the transmitted radiation was collected and concentrated with a semi-spherical condenser before passing to the detector. The IR beam was shaped by the mask slits into a square with side lengths of 15–50 μm. Depending on the IR beam size, each spectrum consisted of 32 to 800 scans with a resolution of 4 cm^{-1}. A scan consisted of one back and forth motion of the mobile mirror in the

https://doi.org/10.1346/CCMN.2013.0610211 Published online by Cambridge University Press

interferometer, which reflects the IR beam to the beamsplitter. The time needed for one scan depends on mirror velocity and the resolution required.

The optical microscope was equipped with an Olympus system. The magnification factor selected for spectra acquisitions was $\times 320$.

Data were sent to the computer and treated using *OMNIC*™ software with *Atlμs* add-on for mapping provided by Thermo Scientific.

The microscope was equipped with a motorized stage which permitted control of both the position and the movement of the thin section in a digitalized X-Y plane with an accuracy of 1 μm. For mapping applications, the motorized stage was used to perform step-by-step acquisition of IR spectra over a selected area. The motorized stage was also programmed for a regular translation to a point set as the background to regularly refresh the background conditions.

Reference transmission FTIR spectra were recorded with 4 cm^{-1} resolution and 100 scan accumulation using KBr sample pellets on a Nicolet 760 FTIR spectrometer equipped with a KBr beamsplitter and DTGS-KBr IR detector.

RESULTS AND DISCUSSION

Effect of sample preparation

The use of IRMS to identify minerals in thin sections is limited in the following ways: (1) the epoxy resin (araldite 2020) which sticks the sample to the glass slide and the resin which impregnates the porous network induces strong absorption bands between 2800 and 3000 cm^{-1} and a broad band at 3400 cm^{-1} (Figure 1a,b). (2) The glass substratum of the thin sections induces strong Si−O absorption which saturates the signal below 2200 cm^{-1} (Figure 1c). As a consequence, IR measurements are available in limited spectral windows, especially in the 3500−4000 cm^{-1} range. This limited range remains of particular interest because it corresponds to the hydroxyl-stretching band region of most clay minerals. (3) Effect of beam size and acquisition parameters on spectrum statistics.

Because IRMS maps of large areas or the use of a small beam size requires the accumulation of numerous scans, the best instrument parameters must be determined for each beam size to optimize spectral quality and minimize data-acquisition time.

To optimize the acquisition conditions for mapping, the effect of the number of scans stacked for a single-point analysis was first studied. An area on the thin section where dickite occurred was selected to better assess the influence of the parameters. The area was selected because no mixing with other minerals was detected in the SEM or FTIR studies.

Spectra recorded after the collection of 100 scans were selected for mapping with a 50 μm × 50 μm window. One hundred scans was a good compromise between spectrum quality and acquisition time as OH-stretching bands of dickite were identified unambiguously and well resolved. For a 25 μm × 25 μm IR beam, the definition of the bands decreased noticeably compared with 50 μm × 50 μm under the same conditions. At least 200 scans were necessary to obtain a well resolved 3710 cm^{-1} band, with a loss of resolution for the bands at 3650 and 3620 cm^{-1}. For a 15 μm × 15 μm window, the smallest window used in this study, the resultant spectra presented incoherent points in absorbance, *i.e.* an oversaturation of the 3620 cm^{-1} band, and

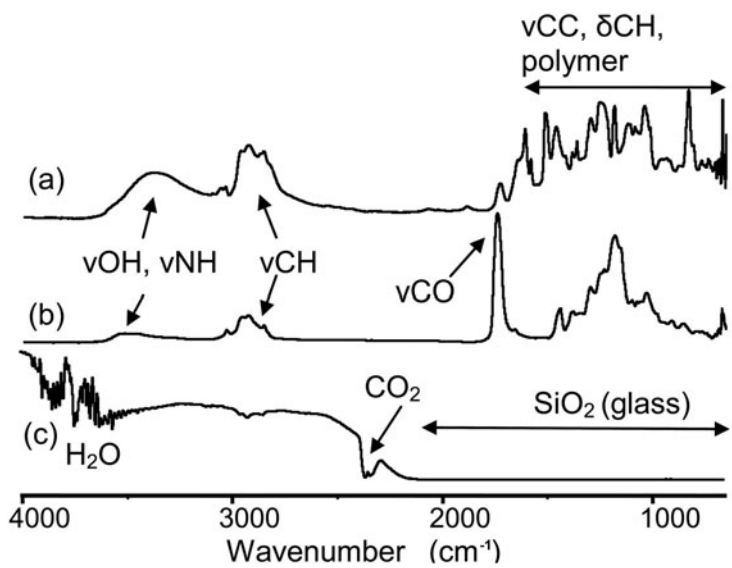

Figure 1. Single-point IR spectra (50 μm × 50 μm beam): (a) epoxy resin used to stick the rock sample on glass slides; (b) epoxy resin used to perform impregnation of porous rock samples; (c) single-channel measurement through air (a glass slide was used as the substratum for thin sections and resin).

https://doi.org/10.1346/CCMN.2013.0610211 Published online by Cambridge University Press

noise-damaged band shapes. At least 800 scans were necessary to get definition good enough for the high wavenumber band near 3710 cm^{-1} for mapping with a 15 μm × 15 μm window. Decreasing the beam size produced a non-linear relationship between spectrum quality and number of scans. The 15 μm × 15 μm beam covered 9% of the surface analyzed with the 50 μm × 50 μm beam (225 and 2500 μm^2, respectively), and 800 scans for the small beam was not enough to reach the same quality as 32 scans for the larger beam (spectra from the 50 μm × 50 μm beam and 32 scans displayed no abnormal points). In order to preserve the same signal to noise ratio, the number of scans for each spectrum needed to be increased exponentially when decreasing the beam size.

Mapping parameters and conditions

The parameters used for mapping acquisition depended on the distance between two successive acquisitions in both the X and Y directions. When an overlap of the analysis windows was selected, the step size used did not exceed 50% of the window size, in order to guarantee an homogeneous covering of the area. The spectra were then processed in order to localize the kaolin polytypes on the map on the basis of the study of the integrated area of specific OH-stretching bands and use of Principal Component Analysis (PCA) as detailed below.

The OH-stretching bands of kaolinite and dickite (3695 and 3710 cm^{-1}, respectively) were used for probing kaolin polytypes in the scanned areas (Figure 3b) because the OH-stretching bands of kaolin minerals occurring at lower wavenumbers were usually overlapped by those of other clay minerals such as micas and chlorite (Figure 2). From an SEM image (Figure 3a), the overlap can be explained by the close contact between the hydroxylated minerals. In such a mapping method, the grayscale level of each pixel of the digital images represented the integrated intensity (*i.e.* area) of bands between 3680 and 3720 cm^{-1} and was proportional to the amount of kaolin minerals contained in the material analyzed (Figure 3c). Smoothing of the raw map was achieved using linear interpolation (Figure 3d). The color scale represented the variation of the integrated intensities from the maximum value (red) and minimum value (blue) calculated. Because parameters were changing from one map to another (beam size, overlap...), integrated intensities also varied. Then a different scale was attributed to each map.

However, in these conditions, direct intensity measurements of absorbance were difficult because of overlapping bands associated with each kaolin polytype (Figure 2) and to unusual intensities of the kaolinite ν_1 bands (Figure 4). Spectra measured from aggregates of small particles were as expected. Spectra with unusual relative intensities of the OH-stretching bands compared to reference kaolinite were specifically recorded for vermicular kaolinite. Acquisition of such an unusual intensity for the kaolinite (particularly ν_1) OH-stretching band has been noted for large vermicular kaolinite from

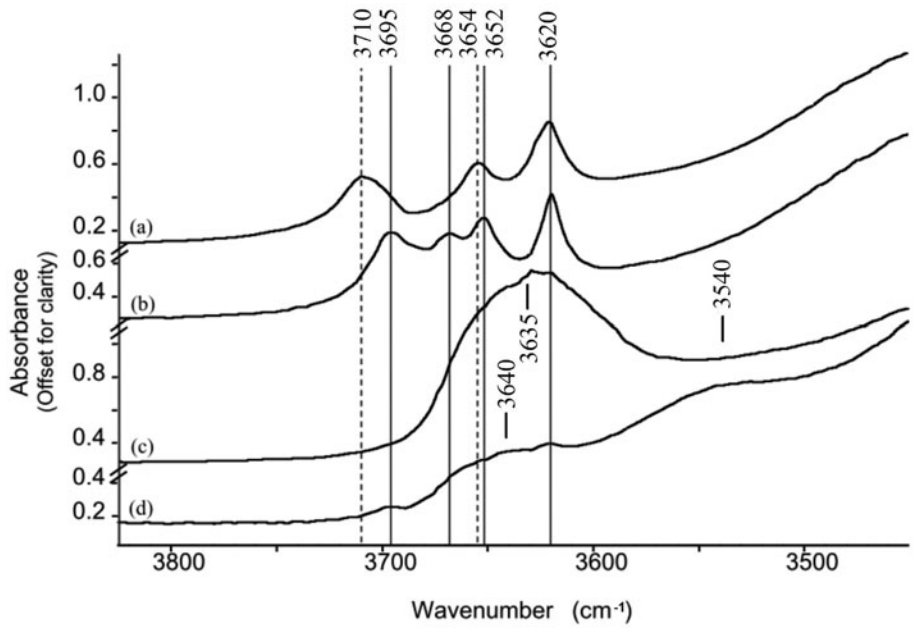

Figure 2. IR spectra in the OH-stretching bands region of phyllosilicates analyzed in the specimen, collected in transmission mode with a 50 μm × 50 μm spot and 100 scans. (a) Dickite, bands at 3710, 3654, and 3621 cm^{-1} (dotted lines); (b) kaolinite, bands at 3695, 3668, 3652, and 3620 cm^{-1} (solid lines); (c) micas, large and intense band centered at 3635 cm^{-1}; (d) chlorite, large bands centered at 3540 and 3640 cm^{-1}, and kaolinite, shoulder at 3695 cm^{-1}. Solid lines represent kaolinite band positions; dotted lines, dickite band positions.

https://doi.org/10.1346/CCMN.2013.0610211 Published online by Cambridge University Press

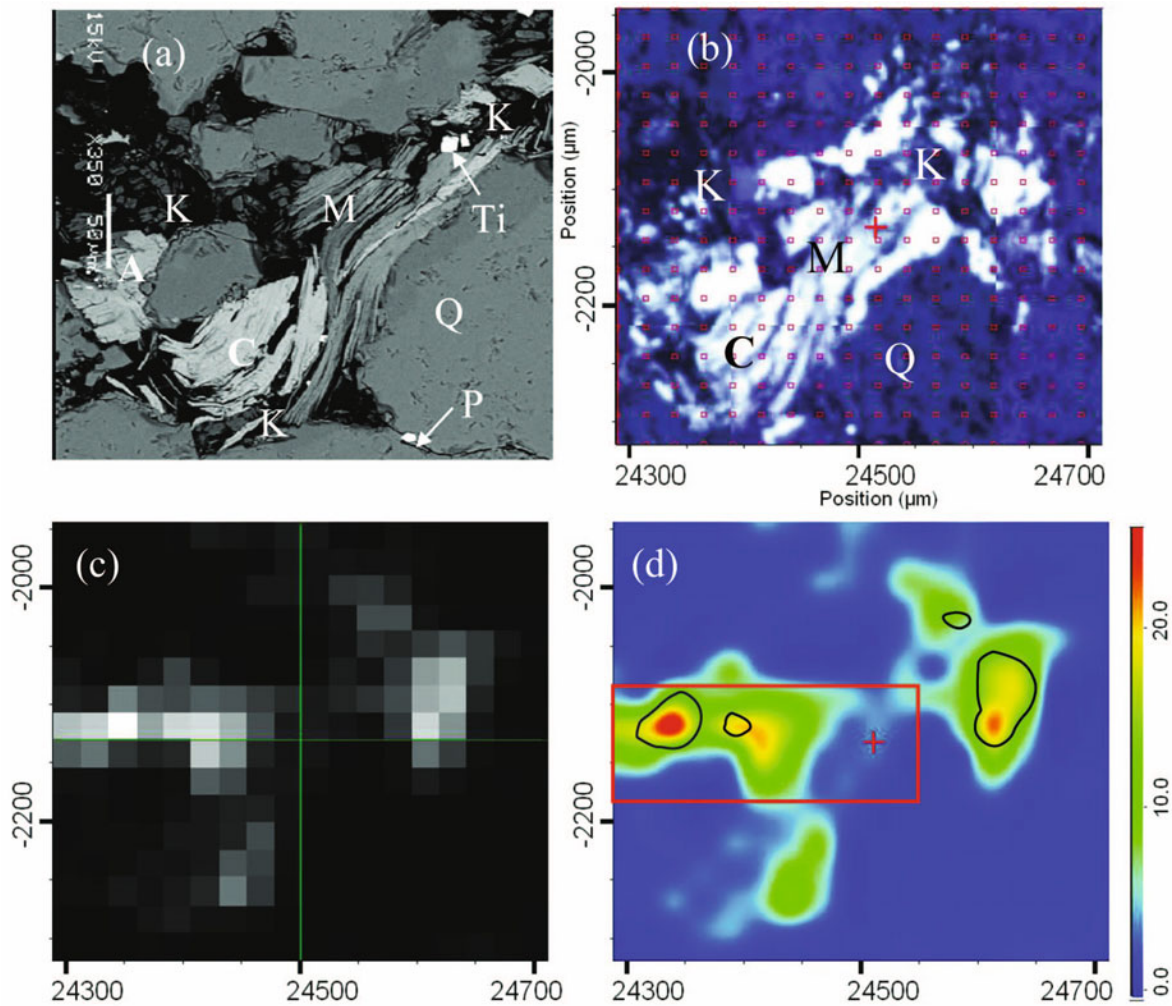

Figure 3. (a) Backscattered electron image. Chemical analysis indicates kaolin minerals (K), mica (M), chlorite (C), ankerite (A), anatase (Ti), pyrite (P), and quartz (Q); (b) optical image of the area of interest from the FTIR microscope digital camera. (c) Map of kaolin minerals, Ib (Table 1) (area shown in parts a and b, 50 µm × 50 µm IR beam and 25 µm step value). Pixels 25 µm × 25 µm, grayscale representing integrated intensity of bands between 3680 and 3720 cm^{-1}. (d) Smoothed map (linear interpolation) of kaolin minerals, with scale of integrated intensities of bands between 3680 and 3720 cm^{-1}. Black contour lines represent dickite-rich areas.

lateritic soils by IRMS (Beauvais and Bertaux, 2002). The unusual relative intensities were interpreted as being due to the large size of vermicular kaolinite giving rise to a very large number of OH vibrators in similar orientations. This constitutes a severe limitation to any quantitative estimation of the respective amounts of kaolinite and dickite from IRMS spectra on textured minerals.

Kaolinite and dickite were distinguished using multispectral Principal Component Analysis (PCA). As described previously, only the bands in the 3690–3720 cm^{-1} range can be used for kaolin minerals characterization (no overlapping with OH-stretching bands of other hydroxylated minerals). As *Atlµs* allows the user to select one or several wavenumber ranges with which the PCA will be done, the multispectral PCA was not applied on the whole MIR range but only on a reduced domain, from 3690 to 3720 cm^{-1}. In this range, *Atlµs* was able to detect the principal components of the spectra, *i.e.* the wavenumber range for which the variance of the absorbance through the whole series of spectra was greatest. Principal components were represented as theoretical bands which were compared to experimental spectra. The degree of correlation between the theoretical bands and the spectra was then used to create a map. The software was used to find the first five principal components. A band close to kaolinite ν_1 was found as the first principal component which was evaluated for correlation with the absorbance of the spectra. The map obtained from the analysis of this first component did not have mineralogical significance; sites with kaolinite or dickite could not be differentiated and almost all sites with OH-stretching absorbance were enhanced. The second principal component found

https://doi.org/10.1346/CCMN.2013.0610211 Published online by Cambridge University Press

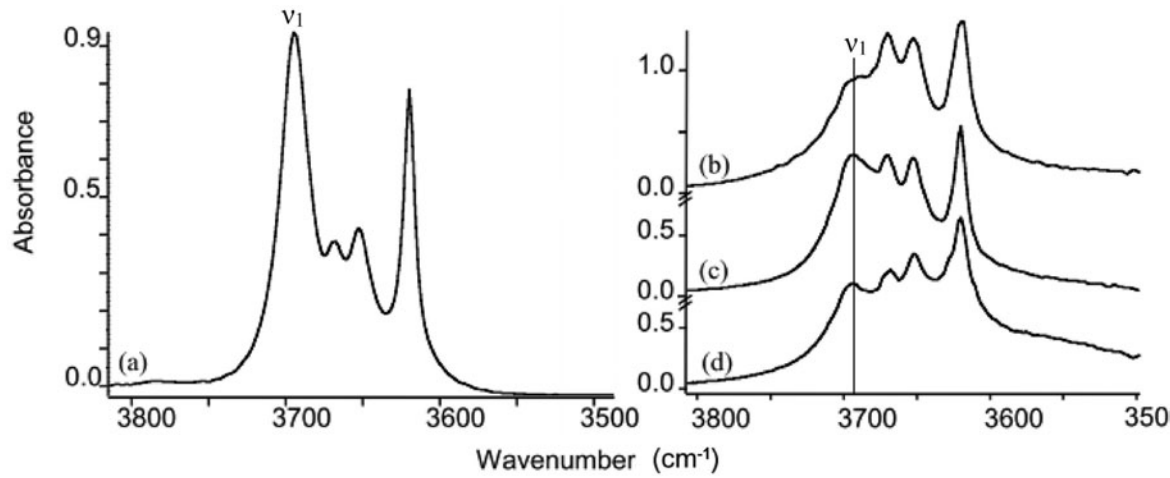

Figure 4. IR spectra of kaolin minerals in the OH-stretching bands region. (a) Kaolinite KGa-1 in KBr pellet; (b, c, d) collected in transmission mode through a 50 µm × 50 µm spot and 100 scans from several locations.

corresponded to the dickite high-wavenumber OH-stretching band. The degree of contribution of the principal component 2 in the recorded spectra was displayed using grayscale on a surface map (Figures 5a, 6c), which gave the locations of the dickite-rich sites. Smoothing of these maps was achieved by using linear interpolation and displayed as color maps (Figures 5b, 6d), using red for spectra with large contributions and blue for spectra with small contributions of the principal component 2. In order to locate the dickite-rich sites on the kaolin minerals maps, a threshold of the dickite maps was created and the contours of the dickite-rich sites displayed as black contour lines on kaolin minerals maps (Figures 3d, 6b). The other principal components after the second were of no mineralogical interest; differentiation between minerals and noise was not achieved.

The IR detector stability had to be monitored over a long period because a mineral map can take several hours to acquire (Table 1). After 16 h of analysis, no drift of the motorized stage and no shift of the condenser alignment were seen. The stability of the detector was monitored, measuring the intensity of the 3710 cm^{-1} IR band of a dickite specimen every 30 min for 11 h. After ~5 h, the intensity of the IR spectrum decreased slightly with increasing time according to a first order equation. However, the loss of intensity measured after 11 h (<5%) was insignificant compared to the intensity values recorded during the acquisition of the maps (Figures 3, 5, 6), and can be ignored for qualitative analysis. If long-time acquisitions are needed, a correction of 0.6%/h can be applied in order to compensate for the intensity loss after 5 h.

Application of FTIR mapping

The results of this methodological work indicate that IRMS can be used to study petrographic thin sections of

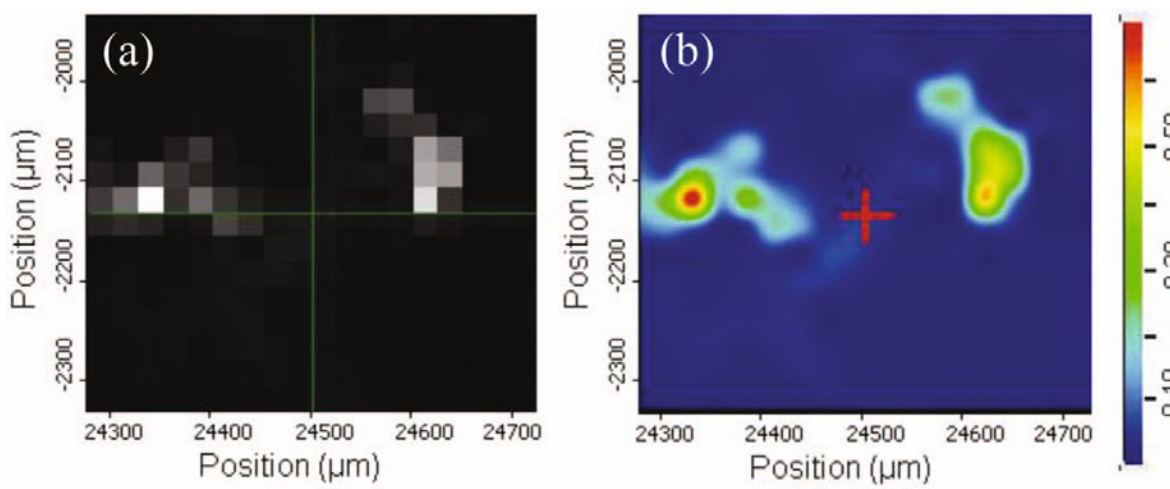

Figure 5. (a, b) Dickite map obtained after PCA applied to map Ib (part c, Figure 6). (a) Dickite map with 25 µm × 25 µm pixels; (b) smoothed map of dickite with color scale.

https://doi.org/10.1346/CCMN.2013.0610211 Published online by Cambridge University Press

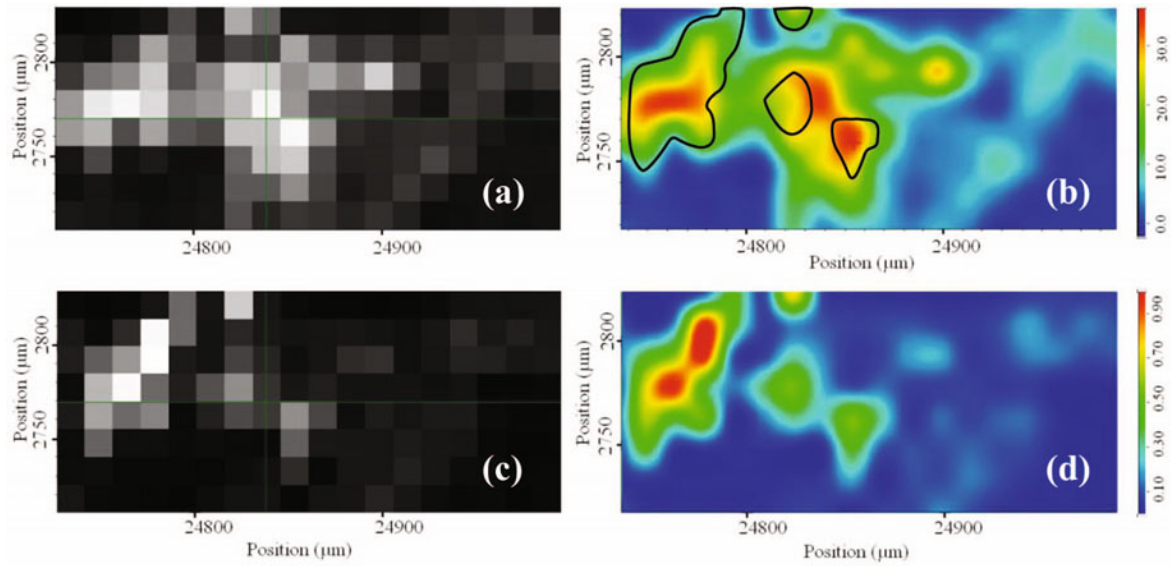

Figure 6. (a, b) Kaolin minerals map III (Table 1). (c, d) Dickite maps. (a) Area X: 24250 to 24550 µm; Y: −2175 to −2275 µm of Figure 3. 15 µm × 15 µm IR beam and 15 µm step value. 15 µm × 15 µm pixels grayscale representing integrated intensities, *i.e.* area, of bands between 3680 and 3720 cm^{-1}. (b) Smoothed map (linear interpolation) of kaolin minerals, with scale of integrated intensities of bands between 3680 and 3720 cm^{-1}. Black contour lines represent dickite-rich areas. (c) Dickite map with 15 µm × 15 µm pixels. (d) Smoothed map of dickite with color scale.

sandstone which suffered kaolinite-to-dickite transition during their burial diagenesis. The IRMS permits (1) the localization of the two kaolin polytypes within the clay cement and (2) the mapping of dickite distribution at the pore scale.

Localizing kaolin minerals in thin section. The main contribution of the IRMS analysis of kaolin minerals in thin section is its ability to characterize each polytype *in situ* in the sandstones (even in the case of small amounts). This is well illustrated in Figure 7. In a previous study, the clay fraction of this sample was extracted and studied by FTIR using KBr pressed pellets. From FTIR spectra of mechanical mixtures of kaolinite and dickite, the dickite/kaolinite ratio was estimated to be 85/15 (Cassagnabère, 1998). Pure kaolinite spectra (Figure 7a) were distinguished from pure dickite (Figure 7d) and mixing of the two kaolin minerals (Figure 7b,c) using IRMS at several locations on the thin section. According to the size of the IR beam used (from 50 µm × 50 µm to 15 µm × 15 µm) and to the SEM observations indicating a <10 µm average size for the crystals of kaolin minerals, most of the single-point analyses collected by IRMS had to be considered as representative of particle aggregates rather than individual particles. The fact that IR spectra of pure kaolinite and/or dickite (Figure 7a,d) had been recorded among spectra corresponding to mixing of the two polytypes of kaolin minerals (Figure 7b,c) indicated that segregations of each polytype exist at a scale which is broadly similar to that of the petrographic observations performed with optical microscopy in thin sections. In other words, the IRMS analysis can be considered as a useful method to complete the petrographic study of thin sections in characterizing the kaolin cement at a relatively local scale (<50 µm × 50 µm). Mapping the kaolin cements with IRMS would allow the easy selection of areas of interest for further *in situ* investigations of each polytype by microprobe analysis or LA-ICP-MS, for instance.

Table 1. Summary of the parameters selected to map kaolin minerals in this study.

Map number	Map dimension (µm)	Beam size (µm)	Scans	Time/step (s)	Step size (µm)	Number of spectra	Total time (h)
Ia	450 × 400	50/50	100	41.83	50/50	90	1.0
Ib	425 × 375	50/50	100	41.83	25/25	288	3.3
Ic	450 × 400	50/50	100	41.83	15/15	868	10.1
II	400 × 350	25/25	200	83.67	25/25	255	5.9
III	260 × 100	15/15	800	334.68	15/15	140	13.5

https://doi.org/10.1346/CCMN.2013.0610211 Published online by Cambridge University Press

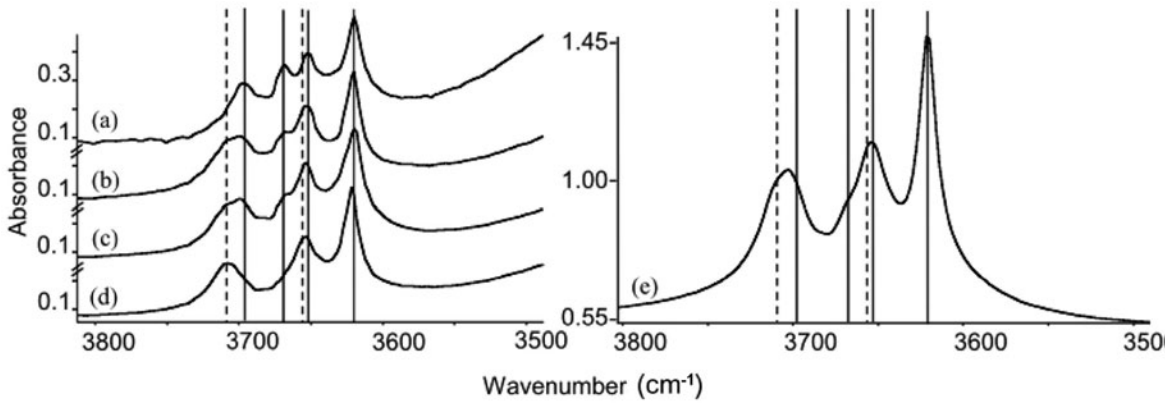

Figure 7. IR spectra of kaolin minerals in the OH-stretching bands region: (a–d) collected in transmission mode through a 50 μm × 50 μm spot and with 100 scans. (e) Extracted clay fraction collected in transmission mode through KBr pellets (Beaufort *et al.*, 1998) (85% dickite and 15% kaolinite, Cassagnabère (1998)). Solid lines represent kaolinite band positions; dotted lines, dickite band positions.

Mapping kaolin minerals. With acquisition time varying with both the window size and the step size value, optimizing the setting parameters in order to minimize acquisition time was crucial. Several maps were created in order to measure the effect of the window size and the step size on the quality of the map (Table 1).

A first map of kaolin minerals (Ib Table 1, Figure 3) was obtained from a thin section in which previous SEM analyses indicated that kaolin minerals, phengitic micas, and Fe-rich chlorite coexist with quartz, ankerite, titanium oxide, and pyrite. This map, in which the size of each pixel was 25 μm × 25 μm (50 μm × 50 μm IR beam with a step size value of 25 μm), confirmed that IRMS allows the identification of kaolin minerals, even in a complex mineral matrix which includes several types of phyllosilicates, with IR absorption in the OH-stretching region (as shown in Figure 2).

Decreasing the step size led to improved detection accuracy of mineralogical variations and a better resolution of the spatial distribution of the minerals investigated (Ia to Ic, Table 1, Figure 8). Map Ia (Figure 8a) was composed of pixels 50 μm × 50 μm in size for a step size value of 50 μm in both the X and Y directions. By decreasing the step value by half in each direction (25 μm) an overlap was created between the areas analyzed and the number of pixels was increased by four (Ib Table 1). The information gain from maps Ia to Ib was significant (Figure 8a,b). In map Ib, strong contrasts were observed within the area represented by one pixel in Ia, showing that the differentiation of dickite within the kaolin minerals was more accurate in Ib than in Ia. The maps III and Ic (Figures 6, 8c), both with the same pixel size 15 μm × 15 μm, displayed a better spatial resolution than the maps Ia and Ib (Figure 8a,b).

If a comparison is made between maps III and Ic (Figures 6, 8c), in which the pixel size was the same but the beam size was different, the quality of the information obtained is notably better in map III (Figure 6). In map Ic (Figure 8c) each pixel represented an average value obtained from several spectra (window size of 50 μm × 50 μm but a step size of 15 μm). In map III (Figure 6) each pixel represented only one spectrum recorded with a 15 μm × 15 μm window size (no overlap of the acquisition windows). The same comparison can be made between the maps Ib (50 μm × 50 μm beam, 25 μm step size) and II (25 μm × 25 μm window size, 25 μm step size) (Figure 8b,c). The spatial resolution and the level of detail were the same, with 25 μm × 25 μm pixels, but the nature of the information was different with an average of several measurements by pixel for map Ib and one spectrum for one pixel for map II.

SUMMARY AND CONCLUSIONS

Infrared microspectroscopy is a convenient method for the characterization of kaolin minerals in sandstone and can be used to study kaolin minerals in their petrographic environment. The method is particularly useful for investigating the petrographic relationships between kaolinite and dickite. Such relationships cannot be examined directly in thin section by other classical methods, such as XRD, microprobe analysis, or SEM observation.

(1) Several authors have proposed that dickite can be distinguished from kaolinite based on crystal morphology (blocky dickite *vs.* vermicular kaolinite). However, IRMS analysis of kaolin minerals with blocky habit indicates that this interpretation is questionable. Indeed, blocky kaolin minerals in a sandstone were characterized as kaolinite using IRMS (Figure 9). Blocky kaolinite in sandstone had previously been identified using EBSD (Kogure *et al.*, 2005), which requires separation and extraction of single crystals before identification. Such methods are not adapted to petrographic examination of thin sections of rocks.

(2) IRMS can be used to map kaolinite and dickite distribution in thin sections at the petrographic scale.

https://doi.org/10.1346/CCMN.2013.0610211 Published online by Cambridge University Press

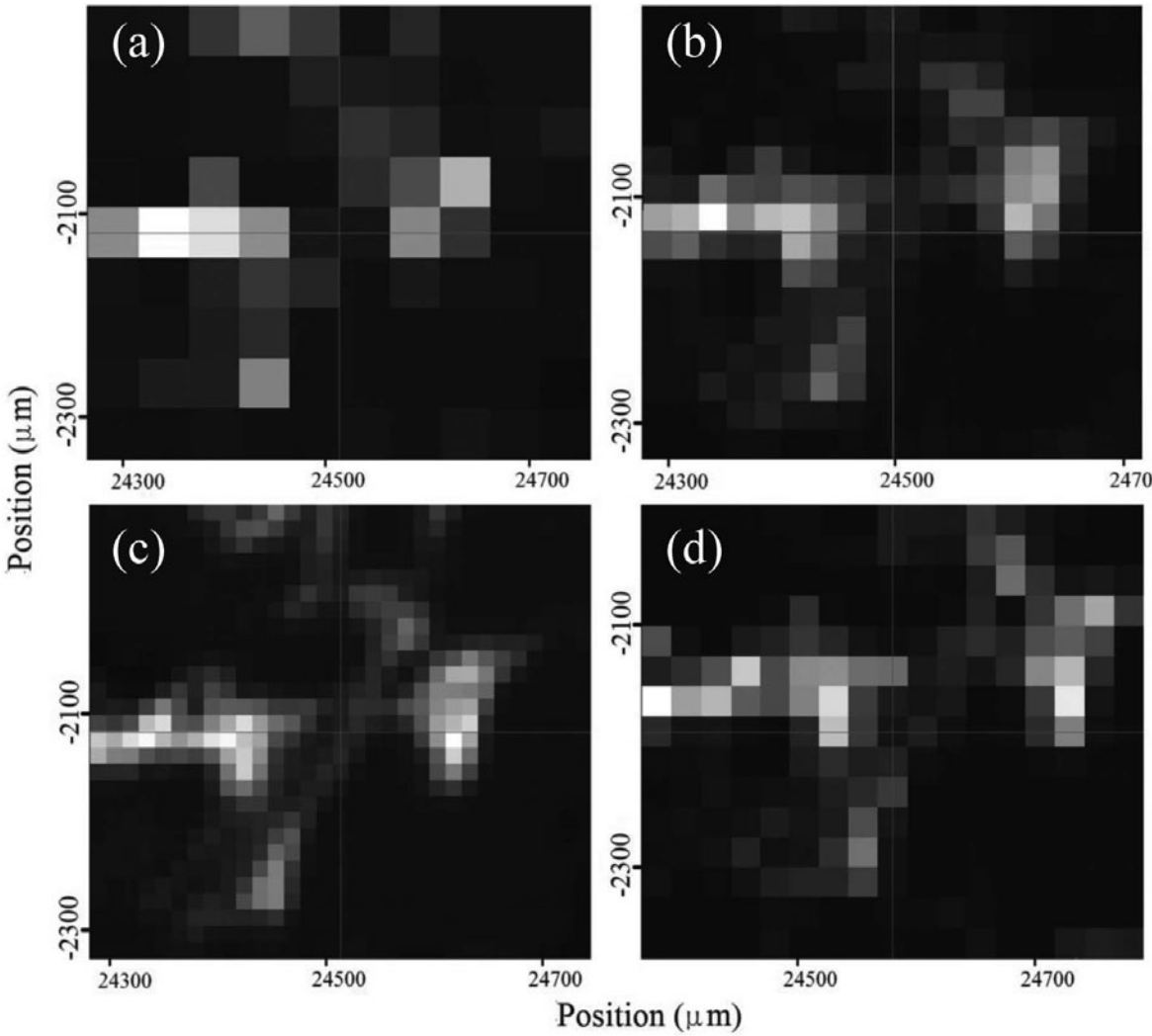

Figure 8. Kaolin map: (a) Map Ia (Table 1), 50 μm × 50 μm IR beam and 50 μm step value in X and Y directions; (b) Map Ib (Table 1), 50 μm × 50 μm IR beam and 25 μm value in X and Y directions; (c) Map Ic (Table 1), 50 μm × 50 μm IR beam and 15 μm step value in X and Y directions; and (d) Map II (Table 1), 25 μm × 25 μm IR beam and 25 μm step value in X and Y directions.

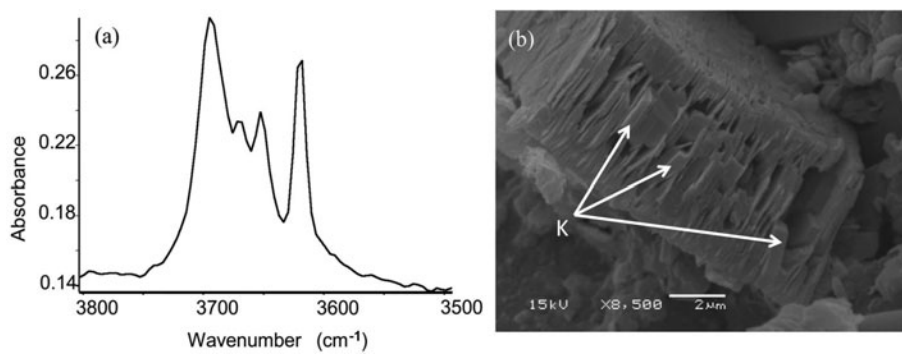

Figure 9. (a) Scale expansion of the OH-stretching region from sample (25_15-1 3006m) collected in transmission mode through a 50 μm × 50 μm spot and with 100 scans. (b) SEM image of intergrowth of kaolin minerals with a blocky habit (k).

https://doi.org/10.1346/CCMN.2013.0610211 Published online by Cambridge University Press

Spatial resolution is limited by the IR window size (15 μm × 15 μm). However, IRMS is particularly well adapted to mapping the distribution of the relatively coarse-grained (up to 30 or 40 μm) kaolinite and dickite formed during sandstone digenesis. Characterization and mapping of other hydroxylated minerals, such as chlorite and micas, can also be carried out using IRMS. However, the spatial resolution of IRMS is minor compared to that of SEM.

(3) Integration of IRMS into a series of petrographic analyses (optical microscope, SEM...) requires the use of thin sections, which have drawbacks, such as glass slide and embedding resin IR interferences, but these interferences can be addressed using self-supporting thin sections (thin sections separated from the glass slide after polishing) and by the use of specific embedding resins.

(4) IRMS can also be used for thin sections of finer-grained kaolin polytypes in other natural environments, such as pedogenic or hydrothermal systems. For example, IRMS has been used to characterize disordered kaolinite in thin sections of soils and to identify structural Fe in the 3598 cm^{-1} absorption band of kaolinite (Beauvais and Bertaux, 2002).

ACKNOWLEDGMENTS

The authors are grateful to the Editor in Chief, Associate Editor, and two anonymous reviewers for their constructive contributions, helping to improve the quality of this paper.

REFERENCES

Balan, E., Saitta, A.M., Mauri, F., and Calas, G. (2001) First-principles modeling of the infrared spectrum of kaolinite. *American Mineralogist*, **86**, 1321–1330.

Balan, E., Lazzeri, M., Saitta, A.M., Allard, T., Fuchs, Y., and Mauri, F. (2005) First-principles study of OH-stretching modes in kaolinite, dickite, and nacrite. *American Mineralogist*, **90**, 50–60.

Balan, E., Delattre, S., Guillaumet, M., and Salje, E.K.H. (2010) Low-temperature infrared spectroscopic study of OH-stretching modes in kaolinite and dickite. *American Mineralogist*, **95**, 1257–1266.

Beaufort, D., Cassagnabere, A., Petit, S., Lanson, B., Berger, G., Lacharpagne, J.C., and Johansen, H. (1998) Kaolinite-to-dickite reaction in sandstone reservoirs. *Clay Minerals*, **33**, 297–316.

Beauvais, A. and Bertaux, J. (2002) In situ characterization and differenciation of kaolinites in lateritic weathering profiles using infrared microspectroscopy. *Clays and Clay Minerals*, **50**, 314–330.

Bish, D.L. (1993) Rietveld refinement of the kaolinite structure at 1.5 K. *Clays and Clay Minerals*, **41**, 738–744.

Brindley, G.W., Kao, C.-C., Harrison, J.L., Lipsicas, M., and Raythatha, R. (1986) Relation between structural disorder and other characteristics of kaolinites and dickites. *Clays and Clay Minerals*, **34**, 239–249.

Cassagnabère, A. (1998) Characterization and interpretation of kaolinite-to-dickite transition in Froy and Rind hydrocarbons reservoirs (North Sea, Norway). PhD thesis, University of Poitiers, France.

De Andrade, V., Vidal, O., Lewin, E., O'Brien, P., and Agard, P. (2006) Quantification of electron microprobe compositional maps of rock thin sections: an optimized method and examples. *Journal of Metamorphic Geology*, **24**, 655–668.

Ehrenberg, S.N., Aagaard, P., Wilson, M.J., Fraser, A.R., and Duthie, D.M.L. (1993) Depth-dependent transformation of kaolinite to dickite in sandstones of the Norwegian continental shelf. *Clay Minerals*, **28**, 325–352.

Farmer, V.C. (1974) *The Infrared Spectra of Minerals*. Monograph **4**, The Mineralogical Society, London.

Farmer, V.C. (1998) Differing effects of particle size and shape in the infrared and Raman spectra of kaolinite. *Clay Minerals*, **33**, 601–604.

Farmer, V.C. and Russell, J.D. (1964) The infra-red spectra of layer silicates. *Spectrochimica Acta*, **20**, 1149–1173.

Frost, R.L. and van der Gaast, S.J. (1997) Kaolinite hydroxyls; a Raman microscopy study. *Clay Minerals*, **32**, 471–484.

Frost, R.L., Tran, T.H., and Kristof, J. (1997) The structure of an intercalated ordered kaolinite; a Raman microscopy study. *Clay Minerals*, **32**, 587–596.

Johnston, C.T., Agnew, S.F., and Bish, D.L. (1990) Polarized single-crystal Fourier-transform infrared microscopy of Ouray dickite and Keokuk kaolinite. *Clays and Clay Minerals*, **38**, 573–583.

Johnston, C.T., Kogel, J.E., Bish, D.L., Kogure, T., and Murray, H.H. (2008) Low-temperature FTIR study of kaolin-group minerals. *Clays and Clay Minerals*, **56**, 470–485.

Kameda, J., Saruwatari, K., Beaufort, D., and Kogure, T. (2008) Textures and polytypes in vermiform kaolins diagenetically formed in a sandstone reservoir: a FIB-TEM investigation. *European Journal of Mineralogy*, **20**, 199–204.

Kogure, T., Inoue, A., and Beaufort, D. (2005) Polytype and morphology analyses of kaolins minerals by electron back-scattered diffraction. *Clays and Clay Minerals*, **53**, 201–210.

Lanson, B., Beaufort, D., Berger, G., Baradat, J., and Lacharpagne, J.-C. (1996) Illitization of diagenetic kaolinite-to-dickite conversion series; late-stage diagenesis of the Lower Permian Rotliegend Sandstone reservoir, offshore of the Netherlands. *Journal of Sedimentary Research*, **66**, 501–518.

Lanson, B., Beaufort, D., Berger, G., Bauer, A., Cassagnabere, A., and Meunier, A. (2002) Authigenic kaolin and illitic minerals during burial diagenesis of sandstones: a review. *Clay Minerals*, **37**, 1–22.

Ledoux, R.L. and White, J.L. (1964) Infrared study of the OH groups in expanded kaolinite. *Science*, **143**, 244–246.

Madejová, J., Balan, E., and Petit, S. (2010) Application of vibrational spectroscopy to the characterization of phyllosilicates and other industrial minerals. *Advances in the Characterization of Industrial Minerals* (G.E. Christidis, editor). EMU Notes in Mineralogy, **9**, European Mineralogical Union and the Mineralogical Society of Great Britain and Ireland, London.

McAulay, G.E., Burley, S.D., Fallick, A.E., and Kusznir, N.J. (1994) Palaeohydrodynamic fluid flow regimes during diagenesis of the Brent group in the Hutton-NW Hutton reservoirs; constraints from oxygen isotope studies of authigenic kaolin and reverse flexural modelling. *Clay Minerals*, **29**, 609–626.

Munoz, M., de Andrade, V., Vidal, O., Lewin, E., Pascarelli, S., and Susini, J. (2006) Redox and speciation micromapping using dispersive X-ray absorption spectroscopy; application to iron in chlorite mineral of a metamorphic rock thin section. *Geochemistry, Geophysics, Geosystems – G³*.**7**, doi: 10.1029/2006GC001381.

Osborne, M., Haszeldine, R.S., and Fallick, A.E. (1994) Variation in kaolinite morphology with growth temperature

in isotopically mixed pore-fluids, Brent Group, UK North Sea. *Clay Minerals*, **29**, 591–608.

Prêt, D., Sammartino, S., Beaufort, D., Meunier, A., Fialin, M., and Michot, L.J. (2010a) A new method for quantitative petrography based on image processing of chemical element maps: Part I. Mineral mapping applied to compacted bentonites. *American Mineralogist*, **95**, 1379–1388.

Prêt, D., Sammartino, S., Beaufort, D., Fialin, M., Sardini, P., Cosenza, P., and Meunier, A. (2010b) A new method for quantitative petrography based on image processing of chemical element maps: Part II. Semi-quantitative porosity maps superimposed on mineral maps. *American Mineralogist*, **95**, 1389–1398.

Prost, R., Damême, A., Huard, E., and Driard, J. (1987) Infrared study of structural OH in kaolinite, dickite, and nacrite at 300 to 5 K. (L.G. Schultz, H. van Olphen, and F.A. Mumpton, editors). International Clay Conference, Denver, 1985. The Clay Minerals Society, Bloomington, Indiana, USA, pp. 17–23.

Prost, R., Dameme, A., Huard, E., Driard, J., and Leydecker, J.P. (1989) Infrared study of structural OH in kaolinite, dickite, nacrite, and poorly crystalline kaolinite at 5 to 600 K. *Clays and Clay Minerals*, **37**, 464–468.

Rintoul, L. and Fredericks, P.M. (1995) Infrared microspectroscopy of bauxitic pisoliths. *Applied Spectroscopy*, **49**, 1608–1616.

Tokiwai, K. and Nakashima, S. (2010) Integral molar absorptivities of OH in muscovite at 20 to 650ºC by in-situ high-temperature IR microspectroscopy. *American Mineralogist*, **95**, 1052–1059.

(*Received 28 August 2012; revised 12 March 2013; Ms. 707; AE: H. He*)